IEEE Access
Multidisciplinary | Rapid Review | Open Access Journal

Received August 5, 2019, accepted August 22, 2019, date of publication August 26, 2019, date of current version September 6, 2019.

Digital Object Identifier 10.1109/ACCESS.2019.2937548

Numerical and Experimental Investigation of Temperature Distribution for Oil-Immersed Transformer Winding Based on Dimensionless Least-Squares and Upwind Finite Element Method

GANG LIU[1], ZHI ZHENG[1], XUN MA[2], SHICHANG RONG[1], WEIGE WU[3], AND LIN LI[4]

[1]Hebei Provincial Key Laboratory of Power Transmission Equipment Security Defense, North China Electric Power University, Baoding 071003, China
[2]State Grid Hebei Electric Power Research Institute, Shijiazhuang 050021, China
[3]Hebei Provincial Key Laboratory of Electromagnetic & Structural Performance of Power Transmission and Transformation Equipment, Baoding 071056, China
[4]State Key Laboratory of Alternate Electrical Power System with Renewable Energy Sources, North China Electric Power University, Beijing 102206, China

Corresponding author: Gang Liu (liugang_em@163.com)

This work was supported in part by the National Key Research and Development Program of China under Grant 2017YFB0902703, in part by the National Natural Science Foundation of China under Grant 51407075, and in part by the Fundamental Research Funds for the Central Universities of China under Grant 2019MS076.

ABSTRACT To accurately analyze the temperature rising and locate the hot-spot of oil-immersed transformer windings, a hybrid method based on the dimensionless least-squares finite element method (DLSFEM) and upwind finite element method (UFEM) is proposed in this paper. To solve the fluid-thermal coupling problem, the sequential iteration method was utilized. After that, the two-side equilibration method and the Jacobi preconditioned conjugate gradient method were used to solve the equations. Moreover, a product-level experimental platform for oil-immersed transformer windings was built. The influence of the turn-to-turn insulation and gravity on the temperature was discussed, and the results show that the influence is significant. To verify the effectiveness of the proposed method, a comparison between the simulation results of the proposed method and experimental results were made, which shows a good agreement. Aiming at verifying the efficiency of the proposed method, the convergence of the proposed method was compared with that of the commercial computational fluid dynamic (CFD) software Fluent. The results indicate that the convergence speed of the proposed method is much faster than that of Fluent, which means a better performance of the new method.

INDEX TERMS Finite element methods, fluid dynamics, numerical simulation, power transformers, temperature measurement, thermal management.

I. INTRODUCTION

As one of the most critical equipment in the power system, the power transformer plays a significant role in the process of power transmission and transformation. The oil-immersed transformer takes oil as medium which has the functions of heat dissipation, insulation and arc suppression; thereby it has found a wide application in different voltage levels and capacities [1].

Due to the high cost of the transformer, its lifespan is one of the most concerned indices and it is affected by many factors, among which the main one is the insulation aging. The local overheating causes the depolymerization of cellulose insulator and reduces the tensile strength and elasticity of cellulose paper, which makes the paper brittle and lose the ability to withstand electric power and mechanical vibration [2], [3]. Once the insulation paper begins to age and to a certain extent, its maintenance is so demanding that it should be replaced as soon as possible. But in fact, the aging paper merely could not be replaced without replacing the winding. Therefore, the lifespan of insulation paper often determines the service life of the transformer. Excessive winding temperature will accelerate the aging of insulation paper, which will greatly shorten the expected life of the transformer [4], [5].

The associate editor coordinating the review of this article and approving it for publication was Mengmeng Li.

Moreover, the local overheating seriously threatens the transformer service life and work efficiency as well, thus it is important to study the problems of winding temperature rising and hot-spot temperature for the safe and stable operation of power systems [6]–[8]. According to the design, the heat dissipation and cooling of transformer are mainly realized by the oil convection, and the oil flow is the greatest factor affecting temperature distribution [9]. Therefore, the essential of the research on temperature rising and hot-spot temperature is to study the fluid-thermal coupling problems of the transformer windings [10]–[14].

Experimental measurement and numerical simulation are the basic means to study these problems. It is imperative to find an accurate and efficient numerical method to analyze the thermal characteristics of the windings.

For the flow and temperature distribution simulation of oil-immersed transformer winding, the generally used numerical methods include finite element method (FEM), finite volume method (FVM) and finite difference method (FDM), etc. The FVM is one of the most popular methods in CFD for its advantages such as good conservation, good numerical stability and strong applicability. However, the numerical convergence of FVM is relatively poor, and the fluid-solid interfaces as well as the wall need to be processed separately. For a boundary-complex, multi-medium model, the computational complexity will be greatly increased [15]. As an efficient and high-precision numerical method, FEM can also solve various CFD problems [16], [17] and ensure the continuity of heat flux density without dealing with the fluid-solid interface separately. It also has good adaptability when dealing with complex boundary, and the calculation accuracy can be improved by changing the interpolation method. However, the numerical stability of the Galerkin FEM is poor and it is prone to non-physical numerical oscillation. In view of this, the most direct approach is to refine the mesh, which results in extra computation amount. Therefore, UFEM was proposed. Based on the weighted residual method of the Galerkin FEM, the weight function of UFEM is not equal to the ordinary interpolation function, but the upwind interpolation function. The upwind interpolation function takes account of the flow characteristics of the fluid and must reflect obvious directionality, so the code of UFEM is much more complex than that of the Galerkin FEM. However, UFEM can effectively eliminate numerical oscillations without extra computation amount [18].

LSFEM is an FEM based on the minimization of the 2-norm of the residuals, which has many advantages of FEM, and makes up for some shortcomings furtherly. The numerical stability of LSFEM is excellent, and the numerical oscillation can be avoided without additional upwind or refining mesh. In addition, the stiffness matrix generated by traditional FEM is not symmetrically positive definite, while the stiffness matrix of LSFEM is a symmetrically positive definite sparse matrix and can be solved by iteration methods. The traditional FEM and the FVM both adopt an indirect coupling method to calculate the velocity-pressure coupling problem, while LSFEM adopts the direct coupling method. Therefore, LSFEM has higher computation efficiency than other methods [19], [20]. However, the governing equations of incompressible fluid are second-order partial differential equations. For LSFEM, the derivative of its base function being the continuous function is required, which makes the issue more complicated. For easy realization in practical engineering, the second-order partial differential equation can be transformed into a first-order partial differential equation by introducing additional variables. It is worth mentioning that the condition number of stiffness matrix is too large due to the great difference of material physical parameters. In view of this, the fluid governing equations were transformed into dimensionless forms [21], [22], and the stiffness matrix was preconditioned when solving the equation [23]. After these processes, the convergence and calculation efficiency of the numerical method can be improved significantly.

LSFEM was applied to the simulation of the flow distribution of four simple examples: the Kovasznay flow, the 2D steady backward-facing step flow, the 3D steady backward-facing step flow and the 2D unsteady circular cylinder flow. The effectiveness of LSFEM was preliminarily verified in solving flow problems, but the heat transfer and fluid-thermal coupling problems still remained unsolved in engineering applications [24]. Furthermore, LSFEM and UFEM were used to simulate the flow and temperature distribution of transformer partial windings. Although the accuracies of the simulation results are considerably satisfactory, the numerical model of winding is too simple to facilitate the realization of the proposed method in which only one pass was set and the effect of insulation paper and gravity on the temperature had not been taken into account. Besides, the tool for method effectiveness verification is Fluent software rather than experimental measurements, which lacks sufficient persuasion [20]. In terms of the efficiency of the method, the conventional LSFEM (dimensional variables in governing equations) was used, and its convergence is poor when solving the fluid-thermal coupling problem [25]. Thereafter, the convergence of conventional LSFEM and DLSFEM was analyzed. The convergence of DLSFEM is much better than that of conventional LSFEM. However, the winding model is too simple and the number of meshes and nodes is so small that it is not sufficient to prove the convergence superiority of DLSFEM in solving complex problems with large stiffness matrices [23].

In this paper, a product-level experimental platform of transformer windings was set up, which included a complete winding temperature rising and cooling loop. Then the DLSFEM and UFEM were used to simulate the oil flow and temperature distribution, in which the turn-to-turn insulation and gravity were considered. The accuracy of the simulation results was verified by the measured ones. Finally, a comparison of the convergence between the DLSFEM and Fluent was made.

II. THEORETICAL BACKGROUND

A. GOVERNING EQUATION

Transformer oil can be regarded as incompressible fluid due to the little variation of its density. Thus, the flow state can be described by the following mass conservation equation and momentum conservation equation:

$$\nabla \cdot \boldsymbol{U} = 0 \tag{1}$$

$$(\rho \boldsymbol{U} \cdot \nabla)\, \boldsymbol{U} + \nabla \boldsymbol{p} - \mu \nabla^2 \boldsymbol{U} = \boldsymbol{f} \tag{2}$$

where $\boldsymbol{U}$ is the velocity vector of transformer oil, ρ is the transformer oil density, p is the fluid pressure, μ is the dynamic viscosity, and $\boldsymbol{f}$ stands for the external force density vector.

The fluid and solid heat transfer of the transformer windings can be described by the energy conservation equation:

$$\nabla \cdot (\rho C_P \boldsymbol{U} T) - \nabla \cdot \lambda \nabla T = S_T \tag{3}$$

where C_p is the oil specific heat capacity, T represents the Kelvin temperature, λ is the oil thermal conductivity, and S_T stands for the heat loss density.

B. DLSFEM DISCRETE FORM

The Navier-Stokes equation of incompressible flow is a second-order partial differential equation. To facilitate the realization of LSFEM, the vorticity $\boldsymbol{\omega}$ is introduced to transform the second-order partial differential equation into a first-order one. The velocity-pressure-vorticity form of the Navier-Stokes equation and the mass conservation equation are obtained, as shown in (4):

$$\begin{cases} \nabla \cdot \boldsymbol{U} = 0 \\ (\rho \boldsymbol{U} \cdot \nabla)\, \boldsymbol{U} + \nabla p + \mu \nabla \times \boldsymbol{\omega} = \boldsymbol{f} \\ \boldsymbol{\omega} - \nabla \times \boldsymbol{U} = 0 \end{cases} \tag{4}$$

The transformer winding can be regarded as an axisymmetric structure without taking the winding sticks and the duct spacers into account. Therefore, the numerical model in the 2D cylindrical coordinates is adopted to study the flow and temperature distribution of the windings. The derivation of the LSFEM discrete form combined with the dimensionless form in 2D cylindrical coordinates is given below.

Firstly, the variables in the equations are converted into dimensionless forms, that is, the dimensionless variables can be obtained by the ratio of basic variables to characteristic variables. The detailed process is given in [21] and [22], and will not be addressed in this paper for the sake of space limitation. The dimensionless forms of (4) in cylindrical coordinates are as follows:

$$\begin{cases} \dfrac{1}{r}\dfrac{\partial (r u_r)}{\partial r} + \dfrac{\partial u_z}{\partial z} = 0 \\ u_r \dfrac{\partial u_r}{\partial r} + u_z \dfrac{\partial u_r}{\partial z} + \dfrac{\partial p}{\partial r} - \dfrac{1}{r \cdot Re}\left(\dfrac{\partial \omega_\theta}{\partial z}\right) = f_r \\ u_r \dfrac{\partial u_z}{\partial r} + u_z \dfrac{\partial u_z}{\partial z} + \dfrac{\partial p}{\partial z} + \dfrac{1}{r \cdot Re}\dfrac{\partial (r \omega_\theta)}{\partial r} = f_z \\ \omega_\theta - \dfrac{1}{r}\dfrac{\partial u_r}{\partial z} + \dfrac{1}{r}\dfrac{\partial u_z}{\partial r} = 0 \end{cases} \tag{5}$$

where r is the radial coordinate, u_r and u_z represent the radial and axial velocity component separately, f_r and f_z are the radial and axial external force density component separately, $Re = \rho UL/\mu$ is the Reynolds number, U is the characteristic length, L is characteristic velocity, and ω_θ represents the vorticity component.

With the gravity term taken into account, the gravitational acceleration g is 9.81m/s^2, and the axial component of external force density vector f_z is fluid buoyancy which is equal to $g(\rho - \rho_{ref})$, ρ_{ref} is the reference oil density; without gravity, $g = 0$ and the external force vector is equal to 0. Equation (5) can be written as a matrix equation:

$$\boldsymbol{A}(\boldsymbol{g}) = \boldsymbol{A}_1 \frac{\partial \boldsymbol{g}}{\partial r} + \boldsymbol{A}_2 \frac{\partial \boldsymbol{g}}{\partial z} + \boldsymbol{A}_3 \boldsymbol{g} = \boldsymbol{f} \tag{6}$$

in which

$$\boldsymbol{A}_1 = \begin{pmatrix} 1 & 0 & 0 & 0 \\ u_r^0 & 0 & 1 & 0 \\ 0 & u_r^0 & 0 & \dfrac{1}{Re} \\ 0 & \dfrac{1}{r} & 0 & 0 \end{pmatrix} \tag{7}$$

$$\boldsymbol{A}_2 = \begin{pmatrix} 0 & 1 & 0 & 0 \\ u_z^0 & 0 & 0 & -\dfrac{1}{r \cdot Re} \\ 0 & u_z^0 & 1 & 0 \\ -\dfrac{1}{r} & 0 & 0 & 0 \end{pmatrix} \tag{8}$$

$$\boldsymbol{A}_0 = \begin{pmatrix} \dfrac{1}{r} & 0 & 0 & 0 \\ 0 & 0 & 0 & 0 \\ 0 & 0 & 0 & \dfrac{1}{r \cdot Re} \\ 0 & 0 & 0 & 1 \end{pmatrix} \tag{9}$$

$$\boldsymbol{f} = \begin{pmatrix} 0 \\ f_r \\ f_z \\ 0 \end{pmatrix} \tag{10}$$

$$\boldsymbol{g} = \begin{pmatrix} u_r \\ u_z \\ p \\ \omega \end{pmatrix} \tag{11}$$

where u_r^0 represents the radial velocity component after previous iteration, and u_z^0 represents the axial velocity component after previous iteration.

The residual function of (6) is constructed, as shown in (12):

$$\boldsymbol{R} = \boldsymbol{A}(\boldsymbol{g}) - \boldsymbol{f} \tag{12}$$

According to the principle of the LSFEM, to minimize the 2-norm of residual function, the following equation should be defined:

$$\boldsymbol{I}(\boldsymbol{g}) = \|\boldsymbol{A}(\boldsymbol{g}) - \boldsymbol{f}\|_0^2 \tag{13}$$

According to the variational method, (13) can be transformed into the following one:

$$2\int_{\Omega}(\boldsymbol{A}\cdot\boldsymbol{g})^{\boldsymbol{T}}(\boldsymbol{A}\cdot\boldsymbol{h}-\boldsymbol{f})\,\boldsymbol{d}\Omega=0 \tag{14}$$

where Ω is the solution domain, and $\boldsymbol{h}$ is the first-order variation of $\boldsymbol{g}$. The quadrilateral mesh is used to divide the solution domain, and the unknown variables in the element can be obtained by interpolation:

$$\boldsymbol{g}=\sum_{n=1}^{n_d}N_n\,(u_n,v_n,p_n,\omega_n)^T \tag{15}$$

where $\boldsymbol{g}$ is the pending vector, n_d is the node number in an element, N_n stands for the interpolating function, and u_n, v_n, p_n, and ω_n are the radial velocity component, axial velocity component, pressure and vorticity of the nth node in the element, respectively.

Let $\boldsymbol{h}=N$, and substituting (15) into (14) yields:

$$\int_{\Omega}(\boldsymbol{A}N_1,\boldsymbol{A}N_2,\cdots,\boldsymbol{A}N_n)^{\boldsymbol{T}}\cdot(\boldsymbol{A}N_1,\boldsymbol{A}N_2,\cdots,\boldsymbol{A}N_n)$$

$$\boldsymbol{G}\boldsymbol{d}\Omega=\int_{\Omega}(\boldsymbol{A}N_1,\boldsymbol{A}N_2,\cdots,\boldsymbol{A}N_n)^{\boldsymbol{T}}\boldsymbol{f}\boldsymbol{d}\Omega \tag{16}$$

where $\boldsymbol{G}$ is the degree of freedom (DOF) vector of the node.

Equation (16) is the discrete equation form of DLSFEM, which can be written as:

$$\boldsymbol{K}\boldsymbol{G}=\boldsymbol{F} \tag{17}$$

where $\boldsymbol{K}$ is the global stiffness matrix and $\boldsymbol{F}$ is right-hand side function.

It can be seen from (16) that the stiffness matrix $\boldsymbol{K}$ formed by the DLSFEM is symmetrical, positive definite and sparse. In addition, unlike the conventional FEMs, the velocity-pressure coupling problem can be solved by the direct coupling when solving the incompressible fluid problem by DLSFEM. The penalty function method is adopted to impose boundary conditions. When solving the equation, the stiffness matrix is preconditioned by the two-side equilibration method [26], and then the Jacobi preconditioned conjugate gradient method is employed to solve the equations [27]. This method can significantly improve the convergence speed of the iterative solution, thereby reducing the computation amount.

C. UFEM DISCRETE FORM

After solving the flow velocity field by DLSFEM, the winding temperature field is calculated by UFEM which has a good numerical stability and can effectively eliminate the non-physical numerical oscillation phenomenon. Equation (3) is discretized by the weighted residual method, and its specific form is as follows:

$$\int_{\Omega}W_i\,(\nabla\cdot(\rho C_P\boldsymbol{U}T)-\nabla\cdot\lambda\nabla T)d\Omega=\int_{\Omega}W_iS_Td\Omega \tag{18}$$

where W_i is the weight function, $i=1,2,\ldots,n$, and n is the node number.

According to the principle of the Galerkin FEM, the weight function is equal to the interpolation function. To prevent numerical oscillation, the upwind form is introduced:

$$W_i=N_i+\frac{\alpha h}{2}\frac{\boldsymbol{U}}{|\boldsymbol{U}|}\cdot\nabla N_i \tag{19}$$

where h is the characteristic length of element, and α represents the upwind correction factor.

The calculation formula of upwind correction factor in (19) is as follows:

$$\alpha=\coth(P_e)-\frac{1}{P_e} \tag{20}$$

where P_e is the Pellet number.

$$P_e=\frac{\rho C_p\,|\boldsymbol{U}|\,h}{2\lambda} \tag{21}$$

The weight function of UFEM can be obtained by (19)-(21). The other derivation process is similar to that of the Galerkin FEM [28]. Finally, the UFEM discrete equation can be obtained:

$$\begin{aligned}\sum_{j=1}^{n}\{\sum_{e=1}^{n_e}\int_{\Omega}[\rho C_pW_i\left(U\cdot\nabla N_j\right)+\lambda\nabla W_i\cdot\nabla N_j]d\Omega\}T_j\\+\sum_{j=1}^{n}\left(\sum_{e=1}^{n_{e1}}\int_{\Gamma}h_fW_iN_jd\Gamma\right)T_j\\=\sum_{e=1}^{n_e}\int_{\Omega}W_iS_Td\Omega+\sum_{e=1}^{n_{e1}}\int_{\Gamma}h_fW_iT_ad\Gamma\end{aligned} \tag{22}$$

where n_e is the total element number, n_{e1} is the element number of the second and third boundary conditions, Γ is the external boundary of the field, T_a is the ambient temperature, and h_f stands for the heat transfer coefficient.

D. NUMERICAL METHOD OF FLUID-THERMAL COUPLING

In this paper, the DLSFEM and UFEM are combined to analyze the flow and temperature fields respectively. The calculation of temperature field requires the parameters obtained from flow field calculation; meanwhile, the temperature also affects the physical parameters of the flow field. Therefore, the sequential iteration method is applied to calculate the fluid-thermal coupling problem. The calculation process is illustrated in Fig. 1, where ε and σ are the convergence criteria; that is, when the residuals of adjacent two steps are less than convergence criteria, the numerical solution can be judged as convergent solution; otherwise, the sequential iteration will continue.

III. EXPERIMENTAL SETUP

In this paper, a product-level experimental platform of temperature rising and cooling for disc-type transformer winding is used to verify the effectiveness of the proposed method.

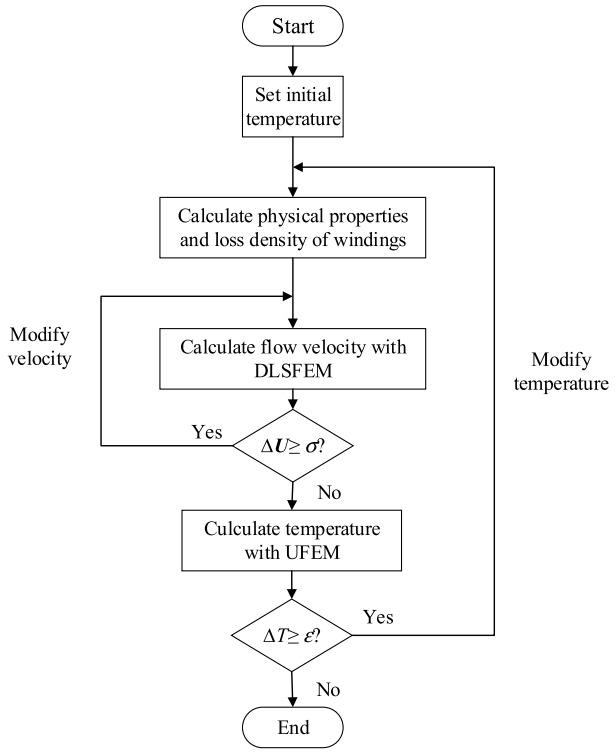

FIGURE 1. Process of fluid-thermal coupling calculation.

The model is mainly composed of the hollow disc-type non-inductive coils, oil tank, radiators, an oil pump, a fan, oil guide tubes, thermocouples and other components. The appearance and sketch graphs of the winding heating and cooling system are shown in Fig. 2.

The inner part of the oil tank of the experimental model consists of the paper-wrapped copper conductor, inner panel, outer panel, guide washer, stick and duct spacer. Fig. 3 is the appearance graph of the winding.

The winding has eight passes. Among them, passes 1-3 contain seven discs, while passes 4-8 contain nine discs. There are 66 discs in all in the winding. The winding is composed of continuous coils, and two coils are connected in parallel, and the wires go out at the terminals. Each disc consists of 15 turns, and each turn of wire consists of two flat copper conductors wound together. In the last disc, the two flat copper conductors are welded together, so that the winding way of the two conductors is the same while the current direction flowing through them is opposite, which results in the offsetting of magnetic field produced by them and the elimination of the eddy current loss of the conductors. Therefore, the loss of the winding after electrification can be considered as resistance loss only. In this way, the loss density under different currents can be obtained accurately. For easy illustration, the passes of winding are numbered from 1 to 8 from top to bottom, and the discs are numbered from 1 to 66 from top to bottom. The flat copper conductors are numbered from 1 to 30 from inner to outer axes.

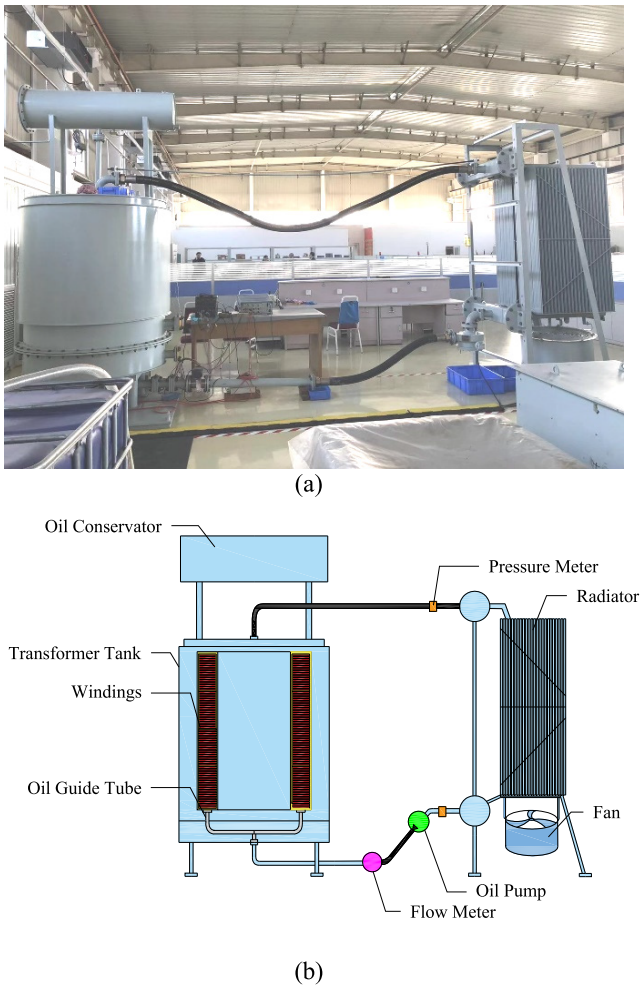

FIGURE 2. Appearance graph (a) and sketch graph (b) of the windings heating and cooling system.

The measurement system of the experimental model consists of a voltage regulator, a precision power analyzer, 45 thermocouples, a liquid turbine flow meter and a temperature logger. The thermocouples are arranged on discs 12, 20, 30 and 38, and 11 temperature measuring points are arranged on each disc, which are located on conductor 1, 4, 7, 10, 13, 16, 19, 22, 25, 28 and 30 respectively. In addition, the thermocouple is arranged at the inlet of the tank to obtain the oil temperature of the corresponding position.

IV. NUMERICAL MODEL

The specific sizes of the model are listed in Table 1. Fig. 4 shows the geometric sketch of the 2D numerical model of windings. The thermocouples on the four discs are placed at the same position. And the thermocouples arranged on Disc 12 are demonstrated in the Fig. 4.

The inlet of the model is taken as the boundary of temperature and velocity. The inlet flux is 25.18m^3/h, the inlet temperature is 57°C, and the calculated inlet velocity is 0.2051m/s. The outlet is the pressure boundary which is 0 Pa·m^2. The insulating cylinder and washer are taken as the

FIGURE 3. Appearance graph of winding.

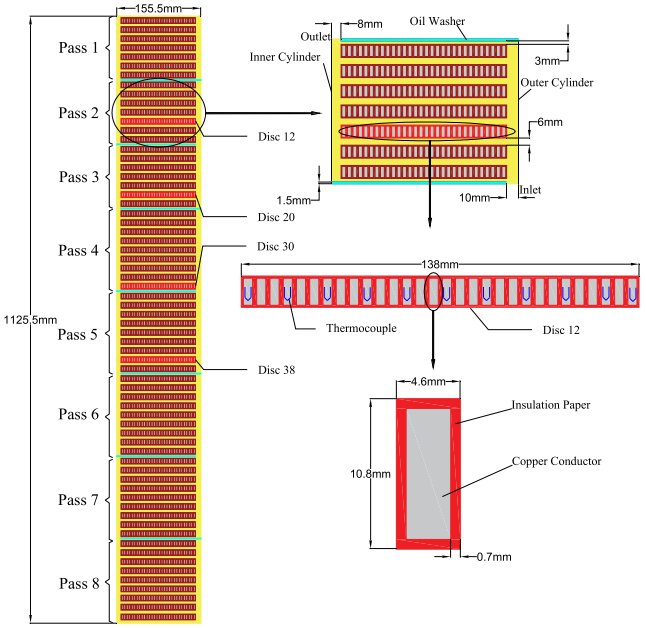

FIGURE 4. 2D numerical model of windings.

TABLE 1. Size of the numerical model.

Item	Size	Value
Total size	Width	155.5mm
	Height	1125.5mm
Disc	Width	138.0mm
	Height	10.8mm
Washer	Width	145.5mm
	Height	1.5mm
Paper	thickness	0.7mm
Horizontal oil duct	Between discs and discs	6.0m
	Between discs and washers	3.0m
Vertical oil duct	Inner axis	8.0mm
	Outer axis	10.0mm

TABLE 2. Material parameters of transformer.

Material	Density ($kg \cdot m^{-3}$)	Thermal conductivity ($W \cdot m^{-1} \cdot K^{-1}$)	Specific Heat ($J \cdot kg^{-1} \cdot K^{-1}$)
Insulation paper	980	0.25	2000
Winding	8960	338	390
Washer	700	0.17	2310

non-slip wall boundaries. The oil tank wall being sealed with double-layer insulation material, it can effectively prevent the increase of insulation material thermal conductivity due to the water absorption, while the thermal conductivity of the insulating cylinders is very small and can be regarded as an adiabatic boundary. The winding loss is considered as the heat source. The power factor of the winding measured by the precision power analyzer is 0.99982, thus it can be assumed that there is only ohmic loss in the winding loss. The power measured by the power analyzer is 56.023 kW. Considering the effect of temperature on the resistance, the equation for calculating ohmic loss with the temperature impact taking into account is as follows [29]:

$$P = P_0 \left[1 + \beta(T - T_0)\right] \tag{23}$$

where $\beta = 0.00393$ is the temperature coefficient of winding for the coil is wounded by the copper conductors, P is the winding loss density, and P_0 is the winding loss density of temperature T_0.

The components involved in the numerical model are transformer oil, disc, insulation paper and washer. It should be pointed out that the physical parameters of transformer oil are greatly affected by temperature and should be expressed by functions of temperature, as shown in (24)-(27). The physical properties of the other material are listed in Table 2.

$$\rho = 1098.7 - 0.712T \tag{24}$$

$$\lambda = 0.1509 - 7.1 \times 10^{-5} T \tag{25}$$

$$C_p = 807.2 + 3.58T \tag{26}$$

$$\mu = 0.0846 - 4 \times 10^{-4} T + 5 \times 10^{-7} T^2 \tag{27}$$

V. RESULTS

A. EFFECTS OF TURN-TO-TURN INSULATION ON TEMPERATURE

As shown in Fig. 4, the insulation paper was so thin that finer meshing of the fluid-solid interface and coil-paper interface was needed to ensure the accuracy of calculation, which leads to a dramatic increase in the number of elements and nodes. Therefore, some researchers simplified the problem by ignoring the turn-to-turn insulation when analyzing the winding temperature rising and hot-spot temperature. However, whether the influence of turn-to-turn insulation on the temperature can be neglected remains to be confirmed.

Therefore, we compare and analyze the flow and temperature distributions through two cases:

I. Models considering turn-to-turn insulation and gravity.

II. Model considering gravity without considering turn-to-turn insulation

It can be seen from Fig. 5 that the difference of flow distribution between case I and case II was not obvious. However, the difference of temperature distribution was significant. The temperature distribution of case II on the same disc was basically average. Moreover, the temperature rising of case I on each disc was significantly higher, and the distinct radial variations of temperature between different conductors of the same disc were found.

Taking disc 12 as an example, the radial temperature variation curves in the two cases are shown in Fig. 6. It can be easily observed that the curve is very smooth for case II. The differences between maximum temperature and minimum temperature were not more than 3°C. In case I, there were distinct radial variations of temperature, and the difference between maximum temperature and minimum temperature was more than 20°C. It can be concluded that the turn-to-turn insulation has a significant influence on the temperature distribution. The turn-to-turn insulation should be considered when analyzing the winding temperature rising and hot-spot temperature.

B. EFFECTS OF GRAVITY ON TEMPERATURE

It is necessary to compare the axial variations of temperature distribution between model with gravity and without gravity for gravity is an axial vector. There is an additional case:

III. Model considering turn-to-turn insulation without considering gravity.

The axial temperature variation curves of case I and III along the vertical center line of the numerical model are shown in Fig. 7. As can be seen, the difference mainly lied in the hottest disc of each pass. The maximum difference was 2.7°C.

The calculated average temperature, hot-spot temperature and hot-spot location on disc 12 in three cases are listed in Table 3. It can be seen that the simulation results of case I were the close to the experimental ones. The simulation results of case II were quite different from the experimental ones, which means the influence of the turn-to-turn insulation on temperature distribution is significant. The simulation results of case III were also in good agreement with the experimental ones. However, as shown in Fig. 7, the effect of gravity on the temperature of the hottest disc in each pass is significant. In summary, neither turn-to-turn insulation nor gravity could be ignored in the simulation of the temperature distribution of windings.

C. VALIDATION OF PROPOSED METHOD

From the analysis above, it can be seen that the influences of turn-to-turn insulation and gravity on temperature

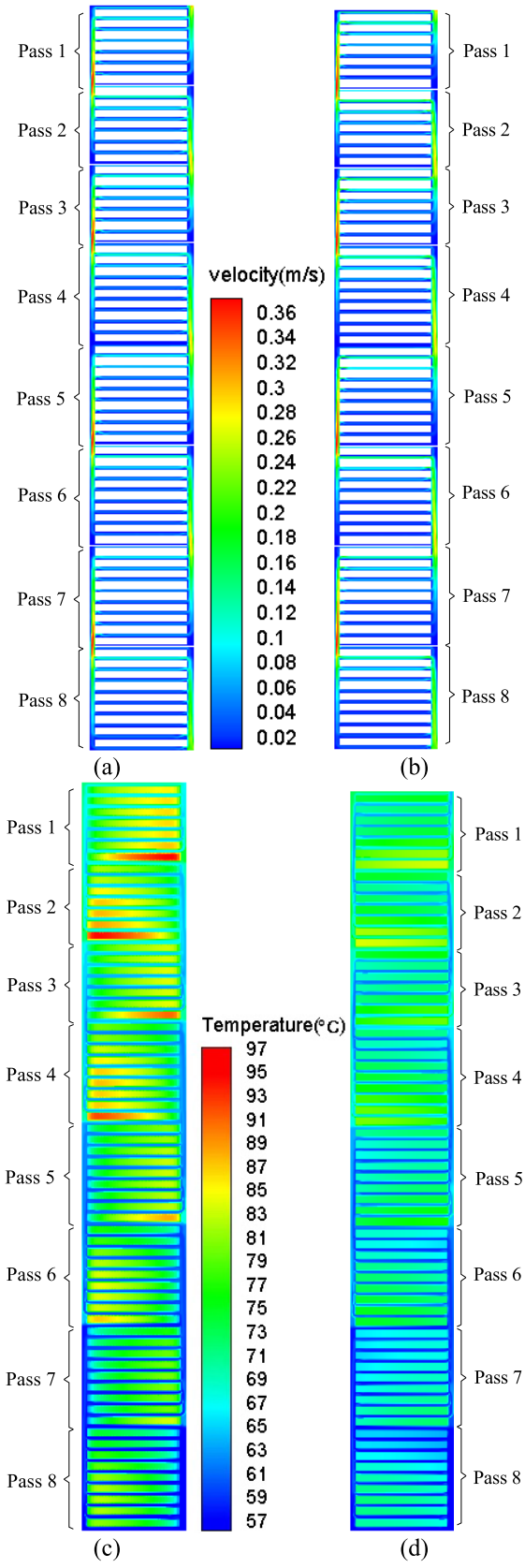

FIGURE 5. Flow and temperature distribution (a, c) with turn-to-turn insulation and (b, d) without turn-to-turn insulation.

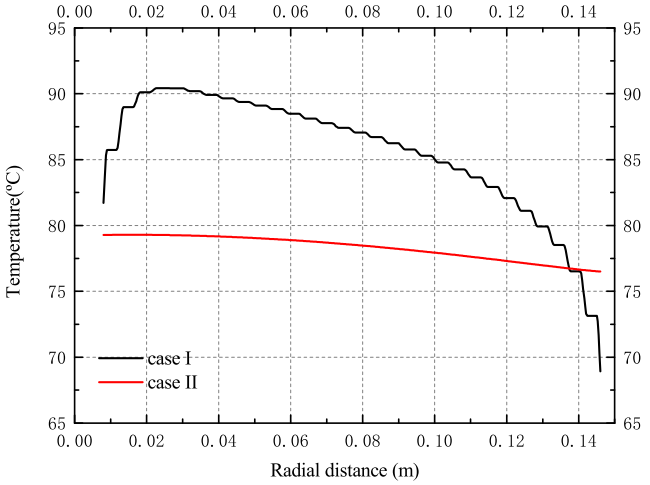

FIGURE 6. Radial temperature curves of disc 12 in case I and case II.

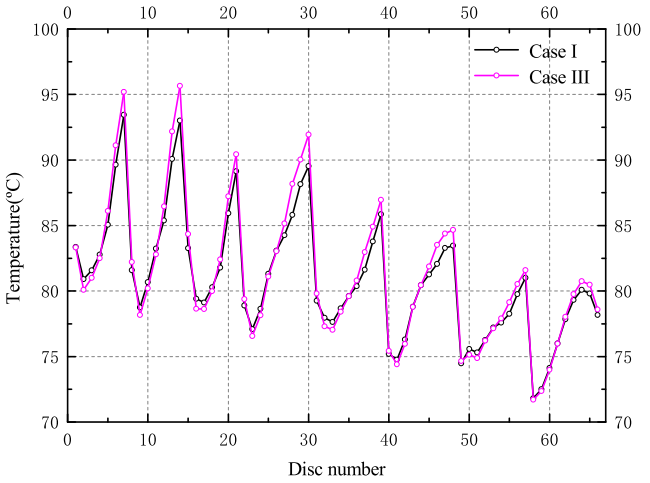

FIGURE 7. Axial temperature curves of disc in case I and case III.

TABLE 3. Average temperatures, hot-spot temperatures and hot-spot locations on disc 12 in three cases.

Case	Average temperature (°C)	Hot-spot temperature (°C)	Hot-spot location
I	84.9	90.2	Conductor 4
II	78.3	79.3	Conductor 1
III	86.3	91.1	Conductor 4
Exp.	85.0	88.8	Conductor 4

rising and hot-spot temperature are particularly significant. If neglected, the simulation error would be large. Therefore, the fluid-thermal field simulation using proposed method was based on the model considering turn-to-turn insulation and gravity. At the same time, the simulation results of Fluent software based on the FVM are given. Fig. 8 and 9 are the flow and temperature distribution contours from pass 2 to pass 5.

From the temperature distribution contour, it can be seen that the hottest disc in each pass is the one close to the washer. Some hot streaks can be observed at these positions.

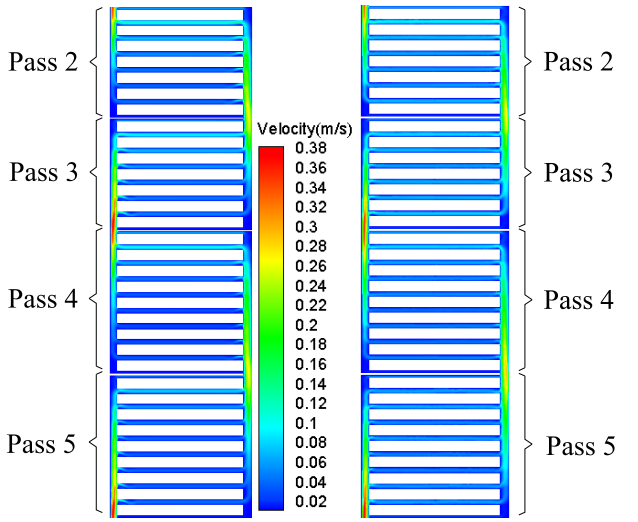

FIGURE 8. Contour of flow distribution obtained by Fluent software (left) and proposed method (right).

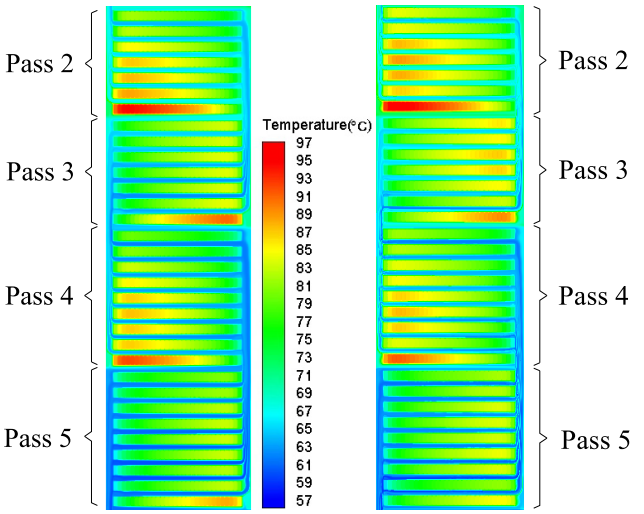

FIGURE 9. Contour of temperature distribution obtained by Fluent software (left) and proposed method (right).

The flow and temperature distribution calculated by the proposed method were basically the same with those calculated by Fluent software, and the difference was not significant. Fig. 10 shows the temperature curves of experimental results and simulation results calculated by the proposed method and Fluent software.

As can be seen from Fig. 10, both the proposed method and Fluent software can approximately simulate the temperature variation on the disc.

Table 4 gives the average temperature and hot-spot temperature of each disc based on the proposed method, Fluent software and experiment. As can be seen from Table 4, due to the turn-to-turn insulation, the radial variation of temperature on the same disc was very large, which makes a distinct difference between the average temperature and the hot-spot temperature. That is the reason why the experimental

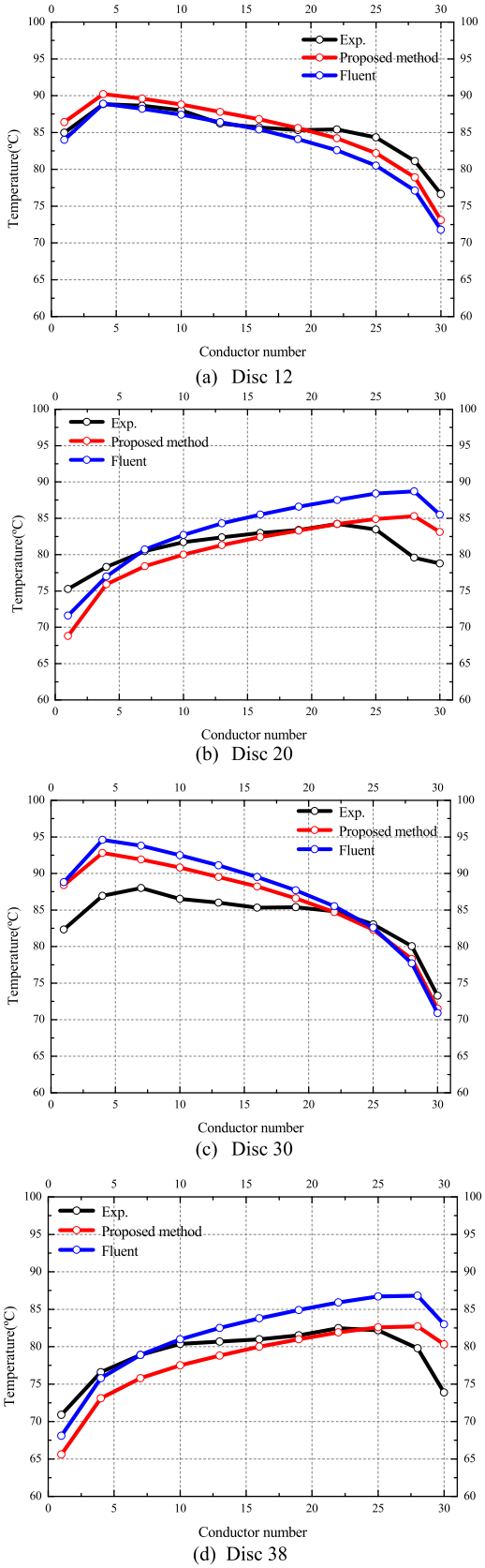

FIGURE 10. Temperature curves of experimental results and simulation results calculated by the proposed method and Fluent software.

TABLE 4. Average temperature and hot-spot temperature of discs.

	Disc number	Proposed method	Fluent	Exp.
Average temperature (℃)	Disc 12	84.9	83.3	85.0
	Disc 20	80.7	83.5	80.9
	Disc 30	85.9	86.8	83.8
	Disc 38	78.1	81.6	78.9
Hot-spot temperature (℃)	Disc 12	84.9	83.3	85.0
	Disc 20	80.7	83.5	80.9
	Disc 30	85.9	86.8	83.8
	Disc 38	78.1	81.6	78.9

measurement in this paper arranged multiple temperature measuring points on one disc. The effectiveness of the proposed method is also verified by the comparison results.

D. ERROR ANALYSIS

There are some differences between the simulation results of the proposed method and those of the Fluent software. The factors causing the differences are as follows:

(1) The proposed method adopts the second-order elements. There are eight nodes in the element for velocity field calculation and nine nodes in the element for temperature field calculation, while Fluent software adopts four-node linear element. Different interpolation methods may lead to different results.

(2) Different from Fluent software based on FVM, the proposed method is based on the DLSFEM and UFEM, so the discretization of equation is different.

(3) Different numerical methods deal with boundary conditions differently. The FVM deals with the fluid-solid interface separately, while the FEM does not.

There are many factors that may lead to the differences between simulation results and experimental ones, and some factors are unavoidable, as stated as follows:

(1) The 2D numerical model does not take into account the influence of sticks and duct spacers on the oil flow and the temperature distribution.

(2) The transition of coil conductor from one disc to another also affects the flow and temperature distribution, which is ignored by the numerical model.

(3) Due to the extrusion effect of external force on the actual model, there exists uncertain compression compared with actual size, that is, the height is not the same with the one given in the blueprints, so there are some differences between the sizes of the numerical model and actual one.

(4) When calculating the parameters, many simplifications had been made for convenience. Therefore, the parameters such as the inlet velocity and loss density used in simulation may be different from those in the actual conditions.

VI. CONTRAST OF CONVERGENCE

In this section, the convergence of the proposed method is compared with that of Fluent. The numerical model of Fluent

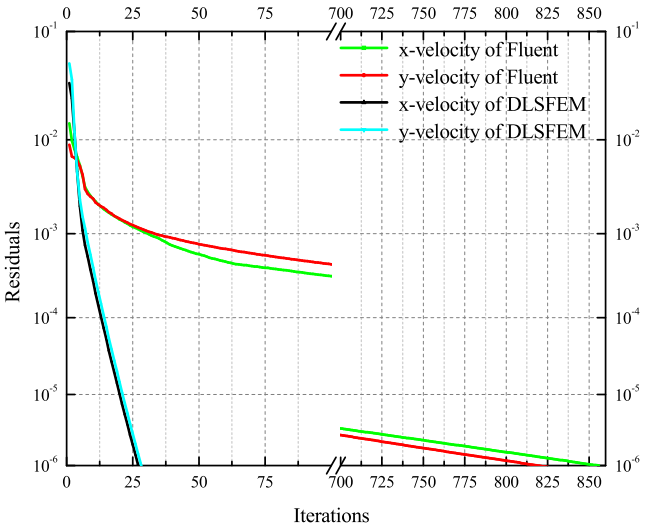

FIGURE 11. Convergence curves.

TABLE 5. Iterative step number of different convergence criteria.

Convergence Criteria	DLSFEM	Fluent
1×10^{-3}	8	34
1×10^{-4}	15	301
1×10^{-5}	22	563
1×10^{-6}	29	856

software was meshed by ICEM CFD software. Quadrilateral elements were selected and the total number of nodes in the whole solution domain was 2,182,489. The numerical model of the proposed method was meshed by ANSYS software. Similarly, quadrilateral elements were selected. The total number of nodes in the whole solution domain was 2,303,993. The convergence curves are drawn in Fig. 11.

Table 5 gives the iteration steps required by the two methods under different convergence criteria. Obviously, the convergence of DLSFEM is better than that of Fluent software, and its iteration steps are much smaller in the meanwhile. The smaller the convergence criterion is, the larger the difference of iteration steps between the two methods is.

VII. CONCLUSION

In this paper, the influence of turn-to-turn insulation and gravity on temperature distribution of transformer windings was analyzed. The temperature rising of transformer winding with considering turn-to-turn insulation was much higher than that of transformer winding without considering inter-turn insulation. Moreover, the hot-spot temperature with considering gravity was significantly lower than that without considering gravity. Therefore, it can be inferred that the influence of both turn-to-turn insulation and gravity on winding temperature should be considered for accuracy of simulation.

Based on the DLSFEM and UFEM, a hybrid method was proposed to analyze the temperature rising and hot-spot temperature of transformer windings. The results calculated by the proposed method were approximately the same as the experimental ones, and the iteration efficiency of the proposed method was much better than that of the Fluent software adopting the FVM, which indicates the superiority of high accuracy and good convergence of the proposed method over other ones.

REFERENCES

[1] Z. Radakovic, M. Sorgic, W. Van der Veken, and G. Claessens, "Ratings of oil power transformer in different cooling modes," *IEEE Trans. Power Del.*, vol. 27, no. 2, pp. 618–625, Apr. 2012.
[2] C. Wang and M. H. Nehrir, "Analytical approaches for optimal placement of distributed generation sources in power systems," *IEEE Trans. Power Syst.*, vol. 19, no. 4, pp. 2068–2076, Nov. 2004.
[3] L. Raeisian, H. Niazmand, E. Ebrahimnia-Bajestan, and P. Werle, "Thermal management of a distribution transformer: An optimization study of the cooling system using CFD and response surface methodology," *Int. J. Elect. Power Energy Syst.*, vol. 104, pp. 443–455, Jan. 2019.
[4] Y. Lin, L. Yang, R. Liao, W. Sun, and Y. Zhang, "Effect of oil replacement on furfural analysis and aging assessment of power transformers," *IEEE Trans. Dielectr. Electr. Insul.*, vol. 22, no. 5, pp. 2611–2619, Oct. 2015.
[5] C. Krause, "Power transformer insulation—History, technology and design," *IEEE Trans. Dielectr. Elect. Insul.*, vol. 19, no. 6, pp. 1941–1947, Dec. 2012.
[6] L. Li, S. Niu, S. L. Ho, W. N. Fu, and Y. Li, "A novel approach to investigate the hot-spot temperature rise in power transformers," *IEEE Trans. Magn.*, vol. 51, no. 3, Mar. 2015, Art. no. 8400204.
[7] *IEEE Guide for Loading Mineral-Oil-Immersed Transformers and Step-Voltage Regulators*, IEEE Standard C57.91, Mar. 2011.
[8] A. Y. Arabul and I. Senol, "Development of a hot-spot temperature calculation method for the loss of life estimation of an ONAN distribution transformer," *Elect. Eng.*, vol. 100, no. 3, pp. 1651–1659, Sep. 2018.
[9] S. Tenbohlen, N. Schmidt, C. Breuer, S. Khandan, and R. Lebreton, "Investigation of thermal behavior of an oil-directed cooled transformer winding," *IEEE Trans. Power Del.*, vol. 33, no. 3, pp. 1091–1098, Jun. 2018.
[10] F. Torriano, H. Campelo, M. Quintela, P. Labbé, and P. Picher, "Numerical and experimental thermofluid investigation of different disc-type power transformer winding arrangements," *Int. J. Heat Fluid Flow*, vol. 69, pp. 62–72, Feb. 2018.
[11] F. Torriano, P. Picher, and M. Chaaban, "Numerical investigation of 3D flow and thermal effects in a disc-type transformer winding," *Appl. Therm. Eng.*, vol. 40, pp. 121–131, Jul. 2012.
[12] F. Torriano, M. Chaaban, and P. Picher, "Numerical study of parameters affecting the temperature distribution in a disc-type transformer winding," *Appl. Therm. Eng.*, vol. 30, nos. 14–15, pp. 2034–2044, 2010.
[13] E. J. Kranenborg, C. O. Olsson, B. R. Samuelsson, L.-Å. Lundin, and R. M. Missing, "Numerical study on mixed convection and thermal streaking in power transformer windings," in *Proc. 5th Eur. Therm.-Sci. Conf.*, 2008, pp. 1–8.
[14] S. B. Paramane, W. Van der Veken, A. Sharma, and J. Coddé, "Effects of oil leakage on thermal hydraulic characteristics and performance of a disc-type transformer winding," *Appl. Therm. Eng.*, vol. 98, pp. 1130–1139, Apr. 2016.
[15] Y. Zhang, S.-L. Ho, W. Fu, X. Yang, and H. Wu, "Numerical study on natural convective heat transfer of nanofluids in disc-type transformer windings," *IEEE Access*, vol. 7, pp. 51267–51275, 2019.
[16] F. Wang, J. Huijian, W. Hao, C. Ziming, T. Jianyu, Y. Yuan, S. Yuhang, and Z. Wenjie, "Radiative, conductive and laminar convective coupled heat transfer analysis of molten salts based on finite element method," *Appl. Therm. Eng.*, vol. 131, pp. 19–29, Feb. 2018.
[17] G.-Y. Jeong, S. P. Jang, H.-Y. Lee, J.-C. Lee, S. Choi, and S.-H. Lee, "Magnetic-thermal-fluidic analysis for cooling performance of magnetic nanofluids comparing with transformer oil and air by using fully coupled finite element method," *IEEE Trans. Magn.*, vol. 49, no. 5, pp. 1865–1868, May 2013.
[18] D. Hendriana and K.-J. Bathe, "On upwind methods for parabolic finite elements in incompressible flows," *Int. J. Numer. Methods Eng.*, vol. 47, no. 1-3, pp. 317–340, Jan. 2000.
[19] B. N. Jiang, "The least-squares finite element method," *Int. J. Numer. Methods Eng.*, vol. 54, no. 10, pp. 3591–3610, 1998.
[20] Y. Xie, L. Li, Y. Song, and S. Wang, "Multi-physical field coupled method for temperature rise of winding in oil-immersed power transformer," *Proc. CSEE*, vol. 36, no. 21, pp. 5957–5965, Nov. 2016.

[21] X. Zhang, Z. Wang, and Q. Liu, "Prediction of pressure drop and flow distribution in disc-type transformer windings in an OD cooling mode," *IEEE Trans. Power Del.*, vol. 32, no. 4, pp. 1655–1664, Aug. 2017.
[22] X. Zhang, Z. Wang, and Q. Liu, "Interpretation of hot spot factor for transformers in OD cooling modes," *IEEE Trans. Power Del.*, vol. 33, no. 3, pp. 1071–1080, Jun. 2018.
[23] G. Liu, Z. Zheng, D. Yuan, L. Li, and W. Wu, "Simulation of fluid-thermal field in oil-immersed transformer winding based on dimensionless least-squares and upwind finite element method," *Energies*, vol. 11, no. 9, p. 2357, Sep. 2018.
[24] T. Sha, Z. Yang, B. N. Jiang, and W. Gu, "Application comparison of least square finite element method and finite volume method in CFD," *Comput. Aided Eng.*, vol. 21, no. 2, pp. 1–6, Mar. 2012.
[25] Y. Xie, "Study on flow field and temperature field coupling finite element methods in oil-immersed power transformer," Ph.D. dissertation, Dept. Elect. Electron. Eng., North China Electr. Power Univ, Beijing, China, 2017.
[26] C.-S. Liu, "A two-side equilibration method to reduce the condition number of an ill-posed linear system," *Comput. Model. Eng. Sci.*, vol. 91, no. 1, pp. 17–42, Feb. 2013.
[27] S. Y. Fialko and F. Zeglen, "Preconditioned conjugate gradient method for solution of large finite element problems on CPU and GPU," *J. Telecommun. Inf. Technol.*, vol. 2, pp. 26–33, Jan. 2016.
[28] B. Zhang, J. Yin, and H. Zhang, "Finite element analysis of typical problems in fluid dynamics," in *Fluid Dynamics Numerical Method*, Beijing, China: Mechanical Engineering Press, 2003, pp. 116–181.
[29] C. Liao, J. Ruan, C. Liu, W. Wen, S. Wang, and S. Y. Liang, "Comprehensive analysis of 3-D electromagnetic-fluid-thermal fields of oil-immersed transformer," *Electr. Power Autom. Equip.*, vol. 35, no. 9, pp. 150–155, 2015.

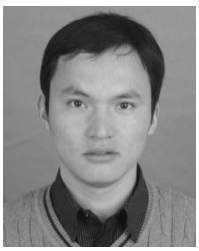

GANG LIU received the Ph.D. degree from the School of Electrical Engineering, North China Electric Power University, Beijing, China, in 2012, where he is currently an Associate Professor. His research interests include the theory and application of electromagnetic field, and simulation and verification of multi-physical coupling problems of electrical equipment.

ZHI ZHENG was born in Hunan, China. He is currently pursuing the master's degree with the School of Electrical Engineering, North China Electric Power University, China. His research interest includes the numerical method and its validity verification of power transformer fluid-thermal field coupling problems.

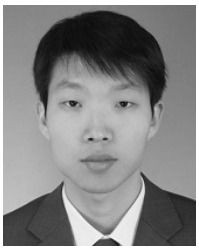

XUN MA was born in Hebei, China. He received the master's degree in electrical engineering and automation from North China Electric Power University, China. He is currently an Engineer with the State Grid Hebei Electric Power Research Institute, Shijiazhuang, China. His research interests include the state grid marketing inspection, anti-stealing specialty, and transformer status analysis.

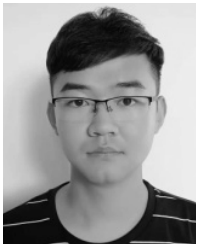

SHICHANG RONG was born in Hebei, China. He is currently pursuing the master's degree with the School of Electrical Engineering, North China Electric Power University, China. His research interests include the efficient method research and verification of the transient electromagnetic-fluid-thermal field coupling problems.

WEIGE WU was born in Hebei, China. He received the master's degree from the School of Electrical Engineering, North China Electric Power University, China. He is currently a Senior Engineer with the Hebei Provincial Key Laboratory of Electromagnetic & Structural Performance of Power Transmission and Transformation Equipment, Baoding, China. His research interest includes calculation and verification of the power transformer's magnetic-fluid-thermal coupling problems.

LIN LI received the B.Sc. and M.Sc. degrees in automation from the Hebei University of Technology, Tianjin, China, in 1984 and 1991, respectively, and the Ph.D. degree in electrical engineering from North China Electric Power University, Beijing, China, in 1997, where he is currently a Professor with the Department of Electrical and Electric Engineering. His research interests include the theory and application of the electromagnetic field and electromagnetic compatibility of power systems.